Journal of the Meteorological Society of Japan, Vol. 91, No. 6, pp. 817–833, 2013
DOI:10.2151/jmsj.2013-607

Aerosol Effects on Cumulus Congestus Population over the Tropical Pacific: A Cloud-Resolving Modeling Study

Xiaowen LI

GESTAR Program, Morgan State University, Maryland, USA
Code 612, NASA Goddard Space Flight Center, Maryland, USA

Wei-Kuo TAO

Code 612, NASA Goddard Space Flight Center, Maryland, USA

Hirohiko MASUNAGA

Hydrospheric Atmospheric Research Center, Nagoya University, Nagoya, Japan

Guojun GU

ESSIC, University of Maryland, College Park, Maryland, USA

and

Xiping ZENG

GESTAR Program, Morgan State University, Maryland, USA
Code 612, NASA Goddard Space Flight Center, Maryland, USA

(Manuscript received 18 September 2012, in final form 6 September 2013)

Abstract

This study examines the significance of aerosol serving as cloud condensation nuclei (CCN) in modulating strengths of tropical maritime convection. Through a Tropical Ocean Global Atmosphere Couple Ocean–Atmosphere Response Experiment (TOGA COARE) case study using a cloud-resolving model (the Goddard Cumulus Ensemble Model with a horizontal mesh interval of 750 m) and a detailed spectral bin microphysical scheme, it is found that low aerosol concentration acts to reduce convection strengths. Over the tropical western Pacific where low-level water vapor is abundant and a ubiquitous weak stable level exists near 0°C, the low background maritime aerosol concentration is conducive for forming cumulus congestus. Sensitivity tests show that the main mechanism of convection damping in a clean maritime environment is through reduced condensational growth, although the freezing of supercooled water, cloud top evaporation, and rain evaporation also contribute to the simulated effects. Considering the importance of congestus in tropical dynamics and the Madden–Julian oscillation (MJO) lifecycle, we further propose a hypothesis that aerosol–cloud–precipitation interactions in an ultraclean marine environment may serve as a damping mechanism for tropical convection.

Keywords aerosol; CCN; cumulus congestus

Corresponding author: Xiaowen Li, Code 612, NASA Goddard Space Flight Center, Greenbelt, Maryland 20771, USA
E-mail: Xiaowen.Li@nasa.gov

1. Introduction

Aerosols in the atmosphere that serve as cloud condensation nuclei (CCN) are crucial for cloud and

rain formation. Aerosols as small as tens of nanometers could serve as CCN, depending on their hygroscopicity and environmental humidity. Human activities generate significant amounts of these aerosols, both directly (e.g., dust, soot, and primary organic carbon) or through gas-to-aerosol conversions (e.g., sulfate, nitrate, and secondary organic carbon). In the past IPCC reports (e.g., IPCC 2007), the single largest uncertainty in human-induced climate change has been associated with how these anthropogenic aerosols affect the Earth's climate through aerosol–cloud–precipitation interactions. Considerable research is devoted to this problem, from both observations and model simulations. While this study builds upon these studies, it focuses on how aerosols serving as CCN modulate convection intensity by changing the cumulus congestus fraction over the ultraclean tropical oceans.

The indirect effects of aerosols on convective clouds are highly uncertain. In addition, the in situ observations of these violent clouds are rare. Remote sensing can be difficult to interpret because of the transient nature of the convection, the difficulties in simultaneously observing aerosol and clouds while separating them unambiguously, and the complications produced by ice phase particles. Cloud-resolving models have simulated both enhancement and suppression in storm intensity due to increasing aerosols (e.g., Tao et al. 2012; Tao et al. 2007; Khain et al. 2008). These simulations included both long-lasting mesoscale convective systems (the PRESTORM and TOGA COARE cases in Tao et al. 2007) and single convective events (the CRYSTAL-FACE case in Tao et al. 2007; all three cases in Khain et al. 2008). Even fewer studies focused on the tropical maritime convection. Several previous studies showed that high CCN concentration may enhance convection intensity and surface rainfall over the tropical oceans. For example, Yuan et al. (2011) linked the enhancement of lightning activity and the convection strength over the western Pacific to increased aerosol loading due to volcanic emissions. Koren et al. (2010) studied deep convective clouds over the tropical Atlantic and found that increased aerosol loading invigorated convection. Moreover, cloud-resolving model simulations of the maritime convection have shown increased storm strengths when CCN concentrations were raised above their background values. Wang (2005) studied the deep convection during the Central Equatorial Pacific Experiment (CEPEX 1993) using a 3D cloud-resolving model with a two-moment microphysical scheme. They found that convection intensity increased with CCN number concentration when the atmosphere was relatively clean. Tao et al. (2007) simulated deep convection during the Tropical Ocean Global Atmosphere Couple Ocean–Atmosphere Response Experiment (TOGA COARE 1992–1993) over the western Pacific warm pool and also concluded that an increase in CCN concentration produced deeper convection and more surface rain. Khain et al. (2008) simulated both the Global Atmospheric Research Program (GARP) Atlantic Tropical Experiment (GATE 1974) and the Large-scale Biosphere–Atmosphere Experiment (LBA 2002) cases and determined that an increase in CCN number concentration from the clean background resulted in enhanced surface precipitation. They concluded that in an environment with high humidity, increased CCN concentration produced more condensational gain than evaporative loss in cloud contents. The net effect was an increase in surface precipitation. van den Heever et al. (2011) conducted radiative–convective equilibrium simulations using a cloud-resolving model with a two-moment microphysical scheme and found that increased aerosol loading strengthened updraft velocities and ice productions, as well as frequencies of the middle clouds. Storer and van den Heever (2013) went on to identify the increase of latent heating as the main mechanism for the enhanced updrafts at lower levels, whereas the increase of hydrometeor loading resulted in weaker updrafts at upper levels. Lebo et al. (2012) demonstrated that increasing aerosol concentration invigorates an idealized supercell storm using both a bin and two-moment bulk microphysical schemes. Their sensitivity tests showed that the increase in latent heating is the key for convection invigoration by aerosols.

Evidence from both observations and modeling studies has shown convection invigoration due to increased aerosol loading, especially in the maritime environment. However, with the exception of van den Heever et al. (2011), previous studies did not specifically address how aerosols (serving as CCN) affected the frequencies of cumulus congestus. Nevertheless, congestus are an important component of tropical convection (e.g., Johnson et al. 1999; Folkins et al. 2008). Recent studies have emphasized their crucial role in moistening mid-troposphere, setting up the optimal condition for deep convective systems, especially in the context of the Madden–Julian oscillation (MJO) lifecycle (Kemball-Cook and Weare 2001; Lin et al. 2004; Kiladis et al. 2005; Tian et al. 2006; Masunaga 2009; Lau and Wu 2010). Environmental factors and physical mechanisms conducive to

the cumulus congestus population over the tropical oceans have been studied by Johnson et al. (1996), Mapes and Zuidema (1996), Folkins et al. (2008), and Folkins et al. (2009). These factors include the relatively small convective available potential energy (CAPE) and the weak stable layer around the melting layer, which is sometimes accompanied by a dry air layer. In this study, we will add an additional factor to these environmental factors. We will demonstrate, through cloud-resolving model simulations, that the lack of aerosols serving as CCN over the clean tropical oceans could promote the formation of congestus.

The paper is organized as follows, Section 2 describes the Goddard cumulus ensemble (GCE) model with an explicit bin microphysical scheme, as well as the environmental and aerosol conditions used in the simulations, Section 3 analyzes sensitivity tests with an emphasis on cloud top heights and cumulus congestus statistics, Section 4 attempts to identify mechanisms of the simulated sensitivities through diagnostic analyses and additional model runs, Section 5 calculates the environment feedbacks produced by different convection types. Finally, Section 6 provides a summary followed by discussions.

2. Model and case descriptions

The GCE model has been developed and improved at the NASA Goddard Space Flight Center over the past 30 years (Tao et al. 2007). The simulations in this study use a similar model setup as described in Tao et al. (2007), which uses the TOGA COARE surface flux parameterization (Wang et al. 2003). For this study, radiation is turned off. Previous simulations with radiation produced similar sensitivities (Tao et al. 2007). All scalar variables use a positive definite advection scheme with a non-oscillatory option (Smolarkiewicz and Grabowski 1990). The simulations in this study are conducted in two dimensions with the open lateral boundaries. The horizontal domain size is more than 2,000 km, with a horizontal resolution of 750 m for the 720 points at the center of the domain. Grids near the lateral boundaries are stretched, and the vertical grids are also stretched with a finer resolution (~80 m) in the boundary layer and coarser resolution (~1000 m) at upper levels. The February 22, 1993 TOGA COARE sounding (shown in Fig. 1) is used as the initial condition for the entire domain. This sounding is a composite of aircraft data below 6 km and an average of the 1800 and 2400 UTC Honiara sounding above 6 km, with 1776 J kg^{-1} CAPE and -3.2 lift index (Trier et al. 1996). This case has been studied extensively by both observations (e.g., Jorgensen et al. 1997; LeMone et al. 1998) and modeling (e.g., Trier et al. 1996; Wang et al. 1996; Tao et al. 2007). A low-level cold pool is applied for the first 10 min in order to initiate the convection. Model sensitivities to the initial cold pool will be discussed in the next section. The total simulation time is 12 h, when the cloud systems have achieved their quasi-steady states, with new convection regenerating steadily in front of the old cell.

The spectral bin microphysical scheme used in the GCE model was developed at the Hebrew University of Jerusalem. Particle size distributions of water drops, six types of ice phase particles (columnar crystals, plate crystals, dendrites, snow aggregates, graupel, and frozen drops/hail), as well as aerosol serving as CCN, are represented by 33 mass size bins for each species. Activations of aerosol in each size bin are explicitly calculated at each time step. Small aerosol particles ($r < 0.03$ μm) are activated into cloud droplets with the equilibrium radius calculated by the Köhler curve. Large particles take much longer to achieve the equilibrium; therefore, they are activated to be five times their dry mass (Khain et al. 2000). The condensational growth rate and environmental supersaturation are solved simultaneously at time intervals smaller than the model time step of 5s, representing a more accurate water vapor budget. Ice nucleation, deposition/sublimation of ice particles, immersion freezing, ice multiplication, melting, drop/drop, drop/ice, ice/ice collision/coalescence, and raindrop collisional breakup are all explicitly simulated in this scheme. Ice nuclei (IN) are specified using Meyers et al. (1992) and are independent of the aerosol concentration in order to focus on the CCN effects. The details of the bin microphysical scheme can be found in Khain et al. (2000).

The main differences between the model setup in this study and that in Tao et al. (2007) are in the representations of the aerosol size spectra. A simple truncated exponential distribution was used in the previous study (Twomey and Wojciechowski 1969). Here the aerosol size distribution is represented by the sum of three lognormal distributions (Jaenicke 1993):

$$n(\log D) = \sum_{i=1}^{3} \frac{N_i}{(2\pi)^{\frac{1}{2}} \log \sigma_i} \exp\left(- \frac{(\log D - \log \overline{D}_i)^2}{2 \log^2 \sigma_i} \right),$$

where D is the particle diameter, N_i, D_i, and σ_i are the specified parameters for different aerosol types. The three modes represent the Aitken, accumulation, and coarse modes of atmospheric aerosols. Figure 2 shows the size distributions of the marine background and

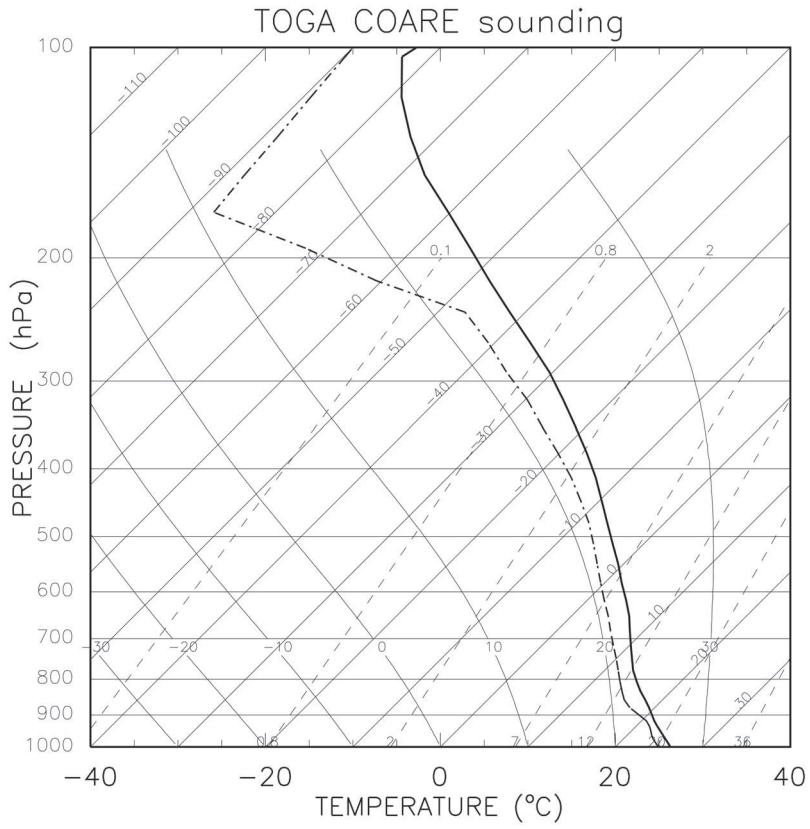

Fig. 1. TOGA COARE sounding used in the simulations. The solid line represents the temperature, and the dash-dotted line represents the dew point temperature.

remote continental aerosols, as used in our sensitivity tests. Aerosol concentration is assumed to be a constant with height for particles with radius smaller than 2 μm. The large particle concentration is constant from the surface to 1 km, and then decreases exponentially with an e-folding factor of 2 km. The sensitivity tests are performed with either a homogeneous or an exponentially decreasing aerosol profile, and the results remain similar (see Section 3.2). For in-cloud aerosol processing in the mixed phase convection, nucleation scavenging is the largest sink term and cloud evaporation/re-suspension is by far the largest source term (e.g., Yin et al. 2005). Nucleation scavenging is explicitly simulated in the model. Re-suspension occurs when cloud droplets completely evaporate. The re-suspended aerosol particle is assumed to have the spectrum of the sum of the accumulation and coarse modes, allowing for a crude representation of the in-cloud aerosol growth. Impact scavenging is not considered in the current simulations; however, it is a sink term for CCN and does not affect conclusions in this study. In addition, aerosols can enter the simulation domain through the lower and lateral boundaries, where the boundary conditions are fixed with the same aerosol spectrum and concentration as the initial condition.

3. Results

The baseline simulations used the original sounding shown in Fig. 1, with a background (clean) and high (dirty) aerosol scenarios. The background aerosol scenario used the background marine aerosol distributions, shown as the solid line in Fig. 2. The high aerosol scenario simply increased the background marine aerosol value by tenfold. The purpose was to preserve the large aerosol tail that is characteristic of marine aerosols (Hudson 1993; Jaenicke 1993). An aerosol scenario with a mean remote continental spectrum was also used for additional sensitivity tests.

Convective systems are highly nonlinear. Both

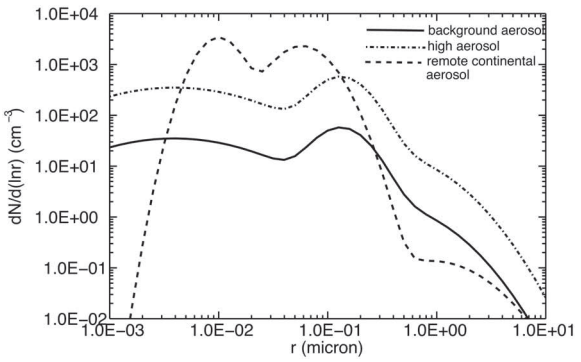

Fig. 2. Aerosol size distributions represented by three lognormal functions. For the background maritime aerosol (solid), N_i = 133, 66.6, and 3.1 cm^{-3}; D_i = 0.008, 0.266, and 0.58 μm; and log σ_i = 0.657, 0.210, and 0.396, respectively, for the three lognormal modes. The high aerosol spectrum in the dash-dotted line increases the background maritime aerosol by 10 folds. For the remote continental aerosol (dashed), N_i = 3200, 2900, and 0.3 cm^{-3}; D_i = 0.02, 0.116, and 1.8 μm; and log σ_i = 0.161, 0.217, and 0.380, respectively.

modeled and observed aerosol indirect effects on convective systems need to establish that the conclusions are statistically significant (e.g., Morrison and Grabowski 2011). This requirement remains a major hurdle in studying aerosol–cloud–precipitation interactions. We attempt to establish the robustness of our model simulation through both the model setup strategy and additional sensitivity tests. First, the case simulated in this study is a long-lived mesoscale convective system. A single sounding was used for the whole domain, with the open lateral boundary conditions and a large horizontal domain. This type of model setup produced a self-regenerating convective system that reached a quasi-steady state after 3–5 h (Rotunno et al. 1988). The quasi-steady states achieved by the models were fairly robust with respect to changes in model resolution (around 1 km) or method of convection initiation (warm bubble vs. cold pool). Second, we performed additional sensitivity tests that varied in initial aerosol spectra and environmental wind shear. The results are reported in Section 3.2.

3.1 Baseline sensitivity tests

Three snapshots of simulated radar reflectivity for both the background and high aerosol scenario are provided in Fig. 3, representing the time evolution of simulated convective systems. The radar reflectivity calculations assumed Rayleigh scattering. In Fig. 3, the left column shows the marine background aerosol case and the right column shows the high aerosol case. Convection is generated quickly by applying a cold pool near the ground for the first 10 min. During the first 90 min, cloud tops remain below 7 km, with no ice formation for both cases. Figures 3a and 3b show the examples of the simulated radar reflectivity at t = 70 min. The system propagates from the left to right, with a new cell forming at the leading edge and an old cell dissipating behind it. Deep convection starts to form after about 100 min. Figures 3c and 3d provide the examples of deep convection in both cases. In general, the high aerosol case has higher cloud tops, more frequent deep convection, and significantly more ice production compared with those of the background aerosol case. The simulations reach their quasi-steady states after 5–6 h. At this stage, all cells for the high aerosol case quickly rise above the 0°C level and produce large amount of ice, whereas significantly less cells do so in the background case, as shown in Figs. 3c–f. Even if they grow deep eventually, they tend to stay at the congestus stage for a much longer time. As a result, the majority of cloud population remains as cumulus congestus in the background aerosol simulation, as opposed to the frequent deep cumulonimbus simulated in the high aerosol case.

The definition of cumulus congestus is not unique. Previous studies used different criteria to define congestus, mainly depending on the observational instruments used (e.g., Johnson et al. 1999, Masunaga et al. 2005, Jensen and Del Genio 2006, Luo et al. 2009). Nevertheless, there are two main physical characteristics of cumulus congestus: 1) the convection is deep enough to rise above the trade inversion and produces significant surface rain (as opposed to the shallow trade wind cumuli) and 2) there are little or no ice phase particles in the convection (as opposed to the deep cumulonimbus). In practice, cumulus congestus clouds are identified by their cloud top heights, which generally center on the melting level (~5 km in the tropics). In this study, we compare results using two different congestus identification methods. Both methods use only the vertical profile information. The first method defines congestus as model pixels with the instantaneous surface rain rate greater than 0.1 mm h^{-1}. In addition, the ice content cannot exceed 1 mg m^{-3} at any pixel along the column. In Fig. 3, the congestus pixels identified by this method are highlighted with hatched lines. This is an adequately accurate way of identifying congestus. One possible error source results from our assumption that the

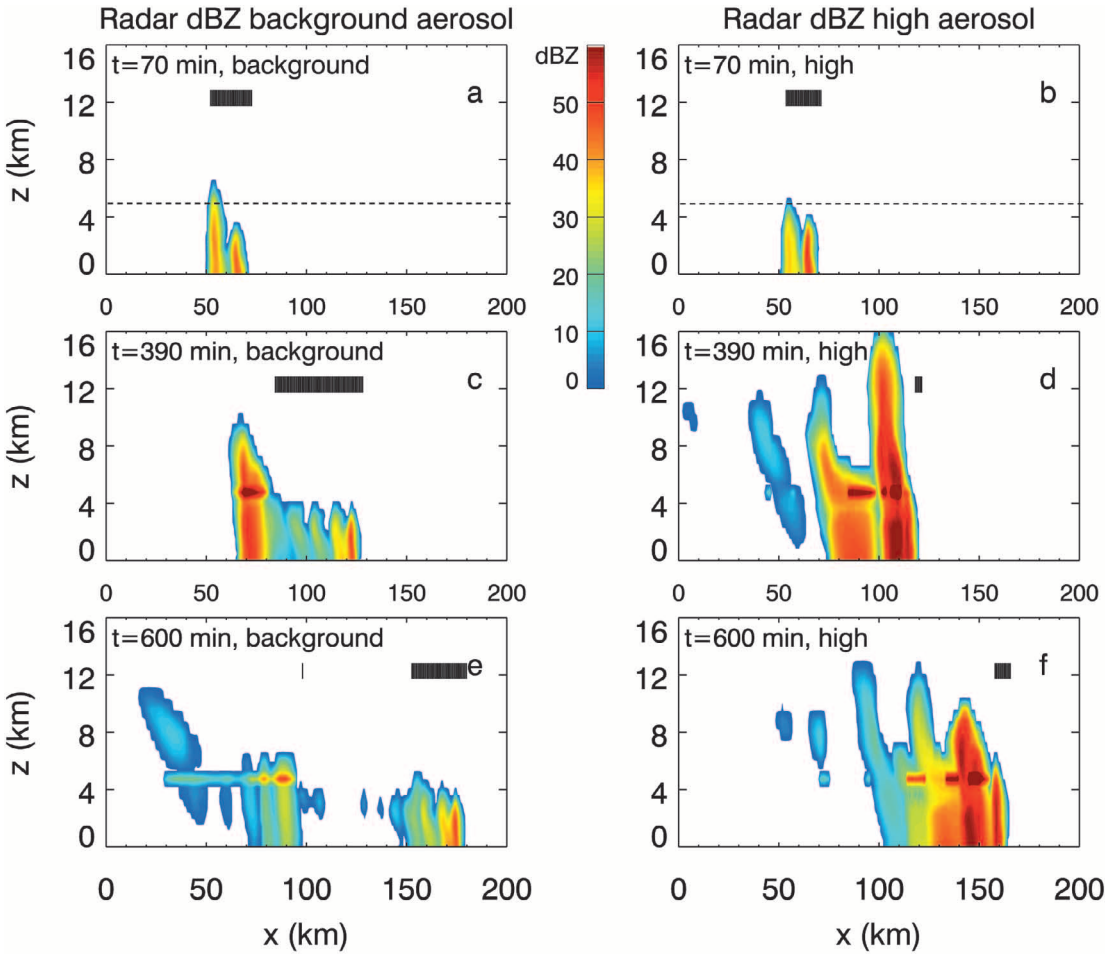

Fig. 3. Snapshots of simulated radar reflectivity (dBZ) for the background (left column) and high (right column) aerosol scenarios. Figs. 3a and 3b: t = 70 min; Figs. 3c and 3d: t = 390 min; and Figs. 3e and 3f: t = 600 min. The dashed lines indicate the melting level. The hatched lines indicate the congestus pixels defined as a point with surface rainfall larger than 0.1 mm h^{-1} and ice phase particle mixing ratio less than 1 mg m^{-3} at any point along the atmospheric column.

clouds are developing vertically, whereas in reality, they often tilt. For example, in Fig. 3e, at x = 100 km, one pixel that belongs to the dissipating stratiform rain is mislabeled as congestus because of the tilting; however, this remains a small error.

The second congestus identification method uses radar observations. The radar reflectivity is simulated using the modeled particle size distributions. The cloud columns with surface radar reflectivity higher than 5 dBZ and with the 0 dBZ (cloud top) heights between 3 and 5 km are defined as congestus. The threshold of 5 km for the cloud top is lower than most of the previous studies (e.g., Jensen and Del Genio 2006); however, when we raise this upper limit, the results tend to overestimate the congestus population by mislabeling some of the dissipating stratiform area as congestus, especially during the quasi-steady state later in the simulation. In the current definition, the differences between the two methods are primarily at the beginning of the simulation, where congestus clouds are mislabeled as deep convection when their cloud top heights surpass 5 km.

Figure 4 shows the time series of the domain-mean surface rainfall rate (Fig. 4a) and the congestus percentage among the raining pixels (Fig. 4b). The thick lines (solid for the background aerosol case and dotted for the high aerosol case) are the results using the first congestus identification method, and the thin lines are

the results using the second method. The domain-mean rain rates indicate that rain initiates earlier for the background aerosol case. In addition, for the initial 100 min, when both cases produce congestus, the background case has slightly higher surface rainfall than the high aerosol case, an indication of higher rain efficiency (e.g., Tao et al. 2007). However, once the deep convection starts to form, the high aerosol case produces significantly larger surface rainfall because of ice production. Moreover, the background aerosol case produces ice but with much less depth and vigor. Therefore, the background case has more than 50% of raining pixels occupied by congestus, whereas the high aerosol case produces mainly deep convection with trailing stratiform anvil, as shown in Fig. 4b.

Figure 5 shows the domain-mean vertical profiles of different hydrometeor species in mass (the mixing ratio in Fig. 5a) and size (the mean diameter in Fig. 5b) for all cloud types. Consistent with Figs. 3 and 4, the high aerosol case has much larger ice water content. Graupel dominates the lower troposphere, whereas pristine ice crystals are the main species at the upper troposphere. There is very little pristine ice (blue lines) in the background aerosol case, where the supercooled water extends to around 9.5 km; for the high aerosol case, it reaches 11 km because the probability of freezing at the same temperature is proportional to droplets' mass. Cloud droplets are smaller for the high aerosol case, as expected from the Twomey effect. Figure 6 further elaborates the simulated cloud droplet size distributions by plotting their averaged spectra. The background aerosol case has a larger mean cloud droplet diameter, with a wider spectrum, compared with the high aerosol case. Because heterogeneous freezing dominates below 11 km, the simulated larger pristine ice in the background case is primarily because of the immersion freezing of larger cloud droplets (Khain et al. 2000). This sensitivity agrees with some previous studies (e.g., Fan et al. 2010; Morrison and Grabowski 2011). The pristine ice grows into snow primarily by aggregation, and the mean snow size is larger for the clean background aerosol case possibly because of the larger initial ice particles. The growth of graupel and hail involves both cloud droplets and raindrops. Although the mean cloud droplet size is larger for the background case, the mean raindrop size is smaller (Fig. 5b). Several mechanisms are possibly responsible for the size distributions of graupel, hail, and rain. For example, larger raindrops in the high aerosol case could form larger embryos for hail. In addition, the high aerosol case has smaller droplets, and these droplets extend higher, allowing for more

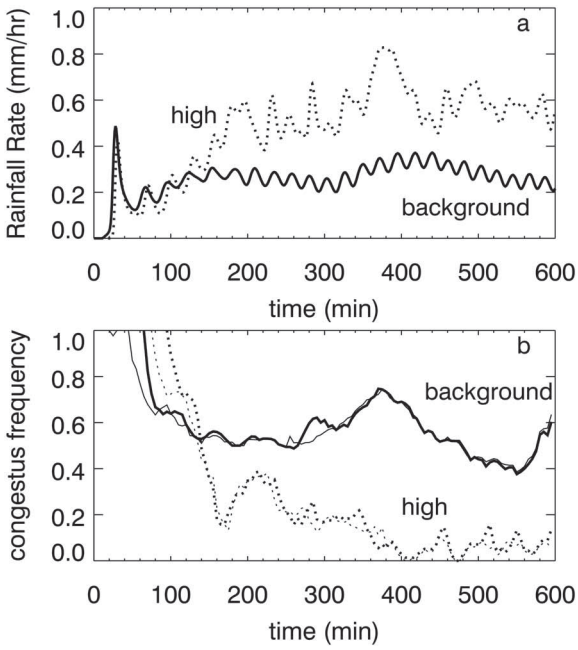

Fig. 4. Time series of domain-mean rainfall rate (a) and congestus frequency among raining pixels (b). The solid lines are for the marine background aerosol case and the dotted lines are for the high aerosol case. For each aerosol scenario, the thick lines use the lack of ice phase particles as the congestus definition, whereas the thin lines use the simulated radar reflectivity and cloud top heights to define congestus.

collection. These could be the reasons for larger hail sizes simulated in the high aerosol case. On the other hand, larger raindrops could occur by melting of larger hail and graupel particles. Graupel often starts from ice/snow aggregates, which then collect cloud droplets. Graupel initially might be larger for the background case because of larger ice/snow aggregates; as they fall and collect both liquid and ice particles, they might grow slower compared with the high aerosol case. Here at least two competing processes are involved in graupel growth.

We have listed several mechanisms that might be responsible for the simulated particle size differences. However, more dedicated studies are required to completely understand how the cloud dynamics and microphysics interact and determine particle size distributions.

3.2 Robustness of the baseline sensitivities

Additional simulations are performed in order to

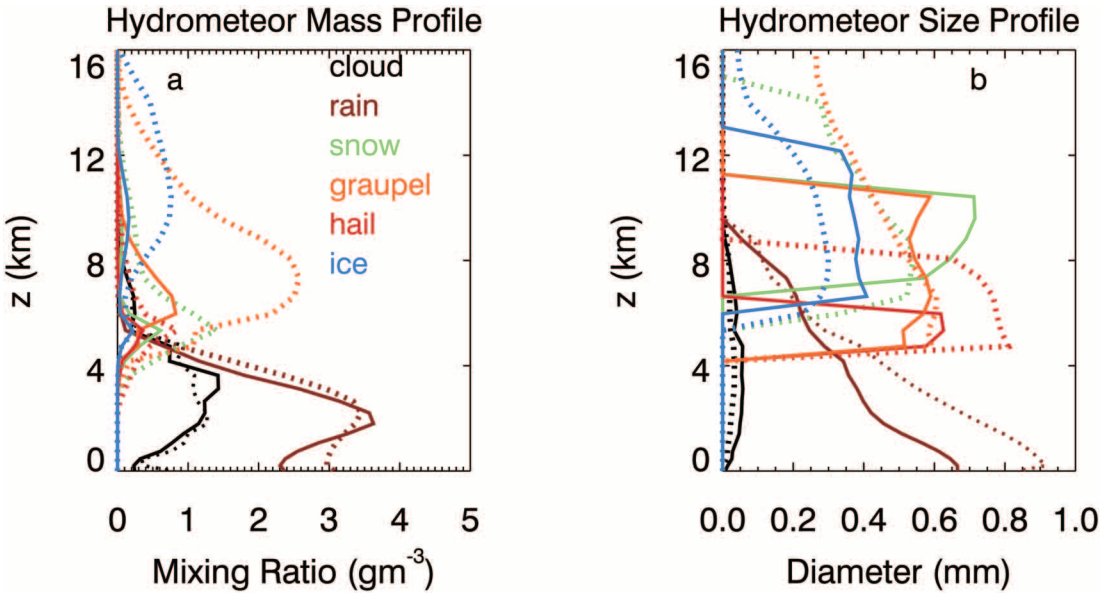

Fig. 5. Domain-mean hydrometeor profiles of (a) mixing ratio and (b) mean particle size over the 10-h simulation period. The solid lines represent the background aerosol case, and the dotted lines represent the high aerosol case. The blue lines represent pristine ice, the green lines represent snow aggregates, the orange lines represent graupel, the red lines are for hail, the black lines are for clouds, and the brown lines are for the rain.

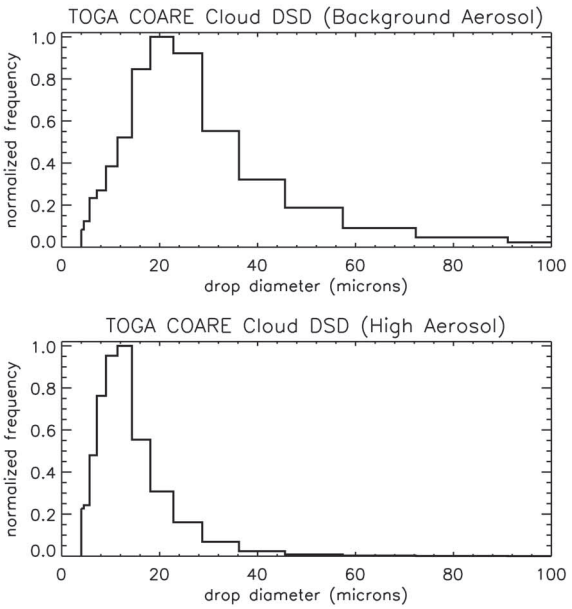

Fig. 6. Normalized, mean cloud droplet size distributions for the background and high aerosol cases.

establish the robustness of convection invigoration by aerosol. These are not the ensemble simulations where large numbers of cases are run with small random perturbations (e.g., Morrison and Grabowski 2011); rather, we seek the confirmation of two different quasi-steady states achieved by high and low initial aerosol concentrations. Each set of experiments differs only in the initial aerosol spectra. The goal is to delineate the robustness of the baseline simulations with a relatively small amount of sensitivity tests because of the high computational cost of running CRM with the explicit bin microphysical scheme.

The convection is initiated using a cold pool between the surface and 3 km for the first 10 min, with a cooling rate of 0.01 K s^{-1}. Our previous simulations have shown some model sensitivities to the strengths of the initial cold pool. In the experiment "cold pool," the cooling rate was increased to 0.02 K s^{-1}, with everything else identical to the baseline cases. The time series of congestus percentages among the raining pixels are plotted as the black lines in Fig. 7. The solid line represents the background aerosol case, and the dashed line represents the high aerosol case. The bifurcated responses during the quasi-steady state are still prominent, with the mean congestus percentage of

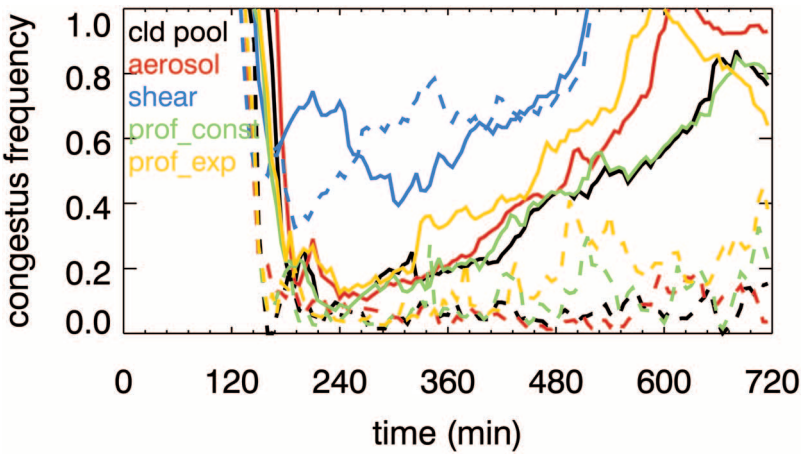

Fig. 7. Time series of domain-mean congestus frequency among the raining pixels. The definition of congestus is according to the presence of ice phase particles. The clean cases are represented by solid lines, and the dirty cases are represented by dashed lines. The black lines (labeled cld pool) double the strengths of the initial cold pool. The red dashed line uses the continental background aerosol to represent a high aerosol environment over the oceans. The red solid line uses half of the mean marine aerosol concentration to represent an ultraclean background. The blue lines increase the vertical wind shear by about 50%. The green and yellow lines vary aerosol vertical distributions, with the green lines using a homogeneous concentration for all particle sizes and the yellow lines have an exponentially decreasing concentration above 1 km.

about 10% for the high aerosol case and more than 50% for the background aerosol case. With a much stronger cold pool, the initial convection remains congestus for a longer period compared with the baseline cases. However, once the deep convection starts, it surges quickly and remains strong with the high aerosol case. In the background aerosol case, the convection slowly weakens to a congestus-dominant state.

In the second set of sensitivity test, the initial aerosol size spectra were varied. Here all environmental settings were kept the same as the black lines in Fig. 7, except for the background aerosol concentration, which was reduced by half to represent an ultraclean maritime environment. The high aerosol case now used the remote continental aerosol spectrum, as shown in Fig. 2, where the large-size tail is reduced compared with the baseline simulation. The results are shown in Fig. 7 by the red lines. Similar to the case "cold pool," perturbing initial aerosol concentrations resulted in the same bifurcation.

Previous studies have shown the important role of low-level wind shear in determining new cell regenerations and the formation of a squall line (e.g., Rotunno et al. 1988, Weisman et al. 2004). Fan et al. (2009) showed that the vertical wind shear could dominate the aerosol indirect effect in deep convection. In the "wind shear" case, we tested a similar idea by increasing the low-level wind shear. In the baseline simulations, the wind speed increases from 0 to 9 m s^{-1} over the lowest 2 km, then gradually reverses to 2 m s^{-1} at 6 km. Above 6 km, the winds center around 0 m s^{-1} with small variations (± 2 m s^{-1}) because the mean wind at mid-troposphere has been removed from the original sounding in order to keep the simulated system centered in the domain. In the sensitivity test "wind shear," the vertical wind was increased uniformly by about 50%, increasing the low-level wind shear from ~4.5 m s^{-1} km^{-1} to about 6.5 m s^{-1} km^{-1} while keeping the mid- and upper-level wind relatively intact. All other variables were identical to the test "cold pool." The results are shown in the blue lines in Fig. 7. In this set of simulations, the model sensitivity to the initial aerosol largely disappeared. For the initial 140 min, both tests exclusively produced congestus. Thereafter, the simulations went into an adjustment period when deep convection and congestus coexisted. After about 500 min, both cases reached a quasi-steady state with congestus as the mode of convection. Note that the precipitation systems with increased low-level wind shear have different characteristics compared with all other simulations in that the

convective system's propagation speed is much faster (~40 km h^{-1}) than the other simulations (~25 km h^{-1}). Fovell and Tan (2000) varied the low-level wind shear systematically and found similar results. Their results pointed to a switch from multicell regime for the low wind shear cases to a unicell regime for the very high wind shear case. In addition, they indicated that the threshold wind shear that governs the switch depends upon different sounding characteristics.

The observations of aerosol vertical distributions remain scarce. Two types of profile were commonly used in model simulations: the exponential and homogeneous profiles. Some evidence suggested that concentrations of large particles had the former profile while small particles had the latter (e.g., Fridlind et al. 2012). The baseline simulations used a combination of these profiles. Additional simulations were conducted to study the model sensitivity on aerosol vertical profiles. The green lines in Fig. 7 represent the sensitivity tests, where the aerosol concentrations were kept constant for all sizes (case "prof_const"). The yellow lines kept constant aerosol concentrations within the lowest 1 km, and then reduced them exponentially above it, with an e-folding factor of 2 km (case "prof_exp"). As shown in Fig. 7, both sensitivity tests have bifurcations in the congestus frequency and support the conclusions from the baseline simulations. Moreover, we notice that the congestus frequency is consistently lower for case "prof_const" than that for case "prof_exp," given the same aerosol concentration near the ground. This may be an indication that CCN entrained from the sides and top of the clouds may also contribute to convection invigoration.

The sensitivity tests show that the convection invigoration by increasing aerosol concentration from the clean marine background level is a robust conclusion for the TOGA-COARE sounding. Furthermore, the single TOGA-COARE sounding used in this study is very similar to the mean sounding during congestus formation taken at the ARM Nauru Island site compiled by Jensen and Del Genio (2006). Nevertheless, the aerosol sensitivity diminished when the low-level vertical wind shear was increased. It remains unclear to what extent aerosol invigorating convection can happen for different environmental conditions over the vast interior of the tropical oceans. More case studies are required in the future.

4. Mechanisms

Several mechanisms have been previously proposed to explain convection invigoration by increasing aerosol loading. In this section, we test these mechanisms systematically, as well as investigate possible new mechanisms, through sensitivity tests and diagnostic studies.

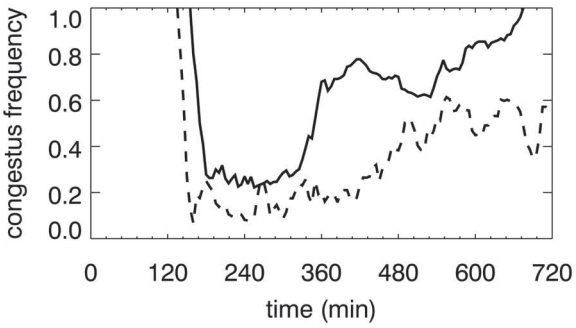

Fig. 8. Same as the "cld pool" case in Fig. 7, except that all ice phase microphysics are turned off. The definition of congestus in this case is according to the simulated radar reflectivity.

4.1 Latent heating through freezing

Perhaps the most popular mechanism for convection invigoration is the freezing of supercooled water (e.g., Rosenfeld et al. 2008). In the high aerosol case, there are more smaller cloud droplets, which reduce cloud collision/coalescence and result in delayed rain formation. More cloud water is carried above the melting level by the updraft compared with the clean background aerosol case. The additional latent heat released by cloud droplet freezing may increase the cloud buoyancy at the upper levels, thus invigorate convection and increase cloud top heights.

In order to verify this, we conducted a set of sensitivity tests, where all the ice phase microphysical processes are turned off. This removes the latent heating by freezing and its feedbacks that may invigorate the convection. The resulted congestus time series are plotted in Fig. 8. After omitting all ice processes, the congestus percentages still bifurcate, albeit to a lesser extent. The high aerosol case has about 40% of congestus compared with only 10% for the "cold pool" case in Fig. 7. The background aerosol case has a mean congestus population of about 80%. The smaller differences simulated in Fig. 8 indicates that freezing does contribute to the convection invigoration. However, on the basis that bifurcation still exists in Fig. 8, we conclude that the freezing mechanism contributes to convection invigoration; however, it is not the determinant factor.

4.2 *Latent heating through condensation*

When the water vapor is abundant but CCN concentration is low, as in the TOGA COARE case, aerosol concentration may become the limiting factor in cloud condensational growth (Reutter et al. 2009). Cloud droplet concentration is low in the marine background case and cannot keep pace with the rapidly increasing supersaturation in the updraft cores. To activate smaller aerosols that have survived the cloud base activation, higher supersaturation is required. Another characteristic of marine convection is that they are very efficient rain producers. Sea spray particles contribute significantly to coarse mode aerosols ($r > 0.5$ μm) (Fitzgerald 1991). These large CCN are activated at relatively low supersaturation and can serve as collectors, efficiently removing small cloud droplets and keeping the cloud droplet concentrations low. Thereafter, the condensational growth rate becomes less compared with a high aerosol scenario where plenty of cloud droplets are available to soak up the supersaturation. Wang (2005) proposed this mechanism for their simulated convection invigoration using a CEPEX case study. In addition, it has been confirmed by Lebo et al. (2012) and Storer and van den Heever (2013).

To test this mechanism, the condensational growth rates are plotted against the in-cloud supersaturation (%), as shown in Fig. 9. For the same in-cloud supersaturation, the condensational growth rate is mostly higher in the high aerosol case (the red triangles). Assuming that all saturated water vapor condenses into cloud droplets (as in the majority of saturation adjustment of the bulk microphysical schemes), the condensational rates vs. supersaturation should align along a straight line, as shown by the dashed line in Fig. 9. When the cloud droplet concentrations are low, the black squares in Fig. 9 generally fall below the idealized line. In this case, the vapor pressure increases to above saturation, sometimes large enough to activate smaller aerosols that have survived the cloud base activation. This is called "in-cloud activation." In this situation, the total latent heat release is reduced, resulting in weaker convection.

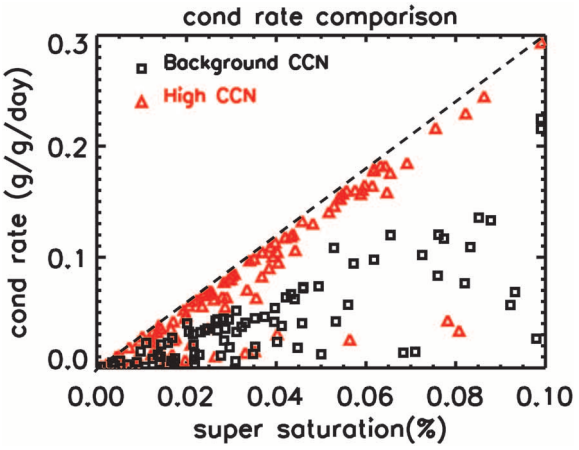

Fig. 9. Condensational growth rate vs. in-cloud supersaturation (%) at 1 km height. Each data point represents the value at one grid cell, between t = 20 min (rain initiation) and t = 60 min. The black squares represent the background aerosol case. The red triangles represent the high aerosol case. The dashed line is the maximum growth rate where all supersaturation is converted into cloud water within one time step. This represents one simple assumption made in some bulk microphysical schemes.

4.3 *Cloud top evaporation*

Over the tropical oceans, the atmospheric instability is relatively low. In addition, a weak stable layer often exists near the 0°C level. The TOGA COARE sounding has both features, with a CAPE of 1776 $m^2 s^{-2}$, and a weak inversion near 5 km. The clouds formed under these conditions may sometimes be considered as successive thermals released from the boundary layer. Each thermal reaches the inversion layer and detrains, cooling and moistening the air at the cloud top, destabilizing the layer, and enabling the next thermal to grow further. Simulated radar reflectivity animations (not shown) demonstrated this behavior. For the high aerosol case, the mean cloud droplet sizes are smaller and cloud water content is higher. Smaller droplets evaporate faster and produce more intense cooling/moistening at its top, destabilizing the cloud top layer more efficiently than the background aerosol case. This allows for more rapid development of deep convection. Once the cloud overcomes the stable layer near 5 km, the atmosphere above it remains neutral or slightly unstable, resulting in deep convection with significant ice productions. The extra heating from cloud droplet freezing in the high aerosol case further enhances the convection.

To illustrate this mechanism, Fig. 10 shows the time series of mean cloud top evaporation rates during the initial cloud development, when both cases have similar cloud top heights and produce congestus exclusively (cf. Figs. 3a and 3b). To calculate the cloud top evaporation rate, we took the cloud top grids where the updraft is more than 1 cm s^{-1}, the cloud water mixing ratio is larger than 1×10^{-4} g m^{-3}, and the air

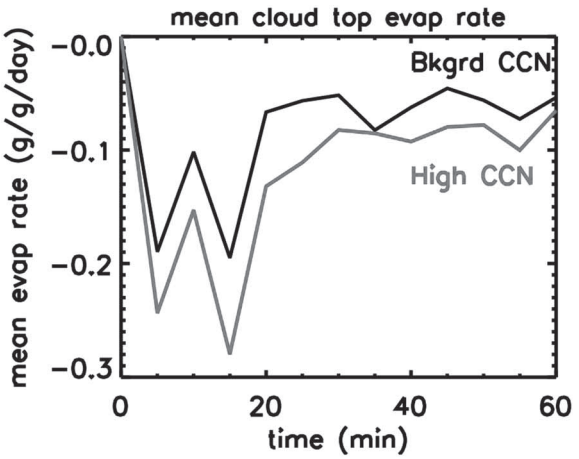

Fig. 10. Variations of mean cloud top evaporation rate with time. Each data point is an average of cloud top grids that are within the updrafts but are sub-saturated due to entrainment. The black line represents the background aerosol case. The grey line represents the high aerosol case.

is sub-saturated. These points represent the grids where the detraining cloud droplets evaporate at the cloud top. These data points are then averaged for each time step. Figure 10 shows that the high aerosol case has a consistently higher cloud top evaporation rate compared with that of the background case, supporting the proposed mechanism. The combination of the reduced latent heating and cloud top evaporation for the background aerosol case keep the convection weaker and lower.

4.4 Rain evaporation

Tao et al. (2007) proposed the mechanism of rain evaporation enhancement according to their model simulations. The convective cell regeneration and propagation are closely related to the cold pool, which in turn is produced and maintained by the storm downdraft and rain evaporation in its outflow (e.g., Rotunno et al. 1988; Weisman et al. 2004). A stronger convection, as simulated in the high aerosol case, is able to induce stronger compensatory downdraft, thus stronger rain evaporation and cold pool. In turn, the stronger cold pool results in stronger secondary convection. While this is not the initial cause of convection invigoration, once the convection becomes stronger, the feedback mechanism helps to maintain it through enhanced secondary convection.

Among the four mechanisms described in this section, the latent heat release through condensation is probably the crucial one. The change in latent heating through freezing can be important when the convection is already deep, but it does not accelerate the transition from congestus to deep convection. The cloud top evaporation mechanism can act independently to facilitate the subsequent convection, whereas the rain evaporation mechanism must act through a positive feedback. Cloud/rain evaporation mechanisms have been inferred from the model data. However, direct proof remains a challenge because evaporation cannot be turned off in the simulations. Nevertheless, our study shows that sophisticated microphysical schemes are required to delineate details of aerosol indirect effects, especially in the representations of vapor condensation and evaporation. The spectral bin microphysical scheme used in this study is a suitable tool. It solves the cloud droplet growth and the environmental supersaturation simultaneously at time intervals one tenth of the model time step of 5s and can be even shorter in the case of strong updrafts (Khain et al. 2008). This represents an accurate water vapor uptake/release by droplets. On the other hand, a bulk microphysical scheme must make assumptions on condensation/evaporation growth. Nevertheless, some of the more sophisticated two-moment bulk schemes, e.g., Wang (2005), Lebo et al. (2012), and Storer and van den Heever (2013), did simulate enhanced condensation due to increased aerosol concentration. Because of the wide range of assumptions made with different bulk microphysical schemes, a bin scheme is generally required to represent various mechanisms described in this section.

5. Feedbacks to the environment

We have shown that aerosol serving as CCN can significantly modulate tropical maritime convection. Using the identical TOGA COARE sounding, the model produces mainly cumulus congestus in a clean background aerosol scenario. When the aerosol concentration increases to a level similar to the remote continental background, the convection invigorates to produce mainly deep convection with trailing stratiform rain. These sensitivity tests offer a unique opportunity to quantitatively study how these two different cloud types affect their environment. Because all simulations began with an identical sounding, we can obtain a clear picture of how different cloud types modify their ambient environments by merely observing the temperature and water vapor profiles after the cloud system passes through.

Figure 11 shows the temperature and water vapor

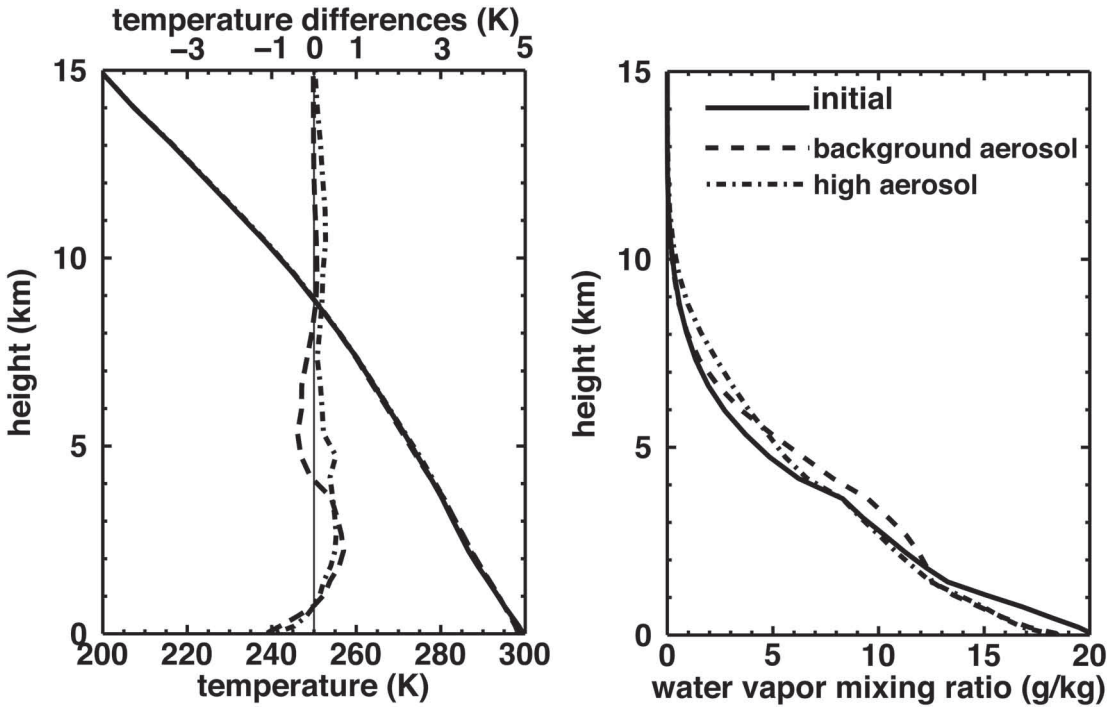

Fig. 11. Mean environmental temperature (left panel) and water vapor (right panel) profiles before and after simulated convective system passage. The solid lines represent the initial profiles, the dashed lines represent the background aerosol simulation, and the dash-dotted lines represent the high aerosol simulation. In addition, temperature profile differences before and after the storm passage are plotted in the left panel (with the axis at the top) in order to show more details.

profiles before and after the convective system passing through a 100 km swath of the model domain. The solid lines represent the initial profiles. At the end of the 10-h simulation, when the model has achieved a quasi-steady state, the profiles in the 100 km domain immediately behind the cloudy area are averaged to represent the mean environmental condition after it is modified by either the congestus or deep convection. The dashed line uses the marine background aerosol, and the dash-dotted line uses the high aerosol scenario. In order to show details, the temperature differences are also plotted with the x-axis labeled at the top of the frame. Both simulations stabilize the lower atmosphere by cooling near the surface and warming between 1 and 4 km. However, the congestus cools the mid-troposphere between 4 and 8 km, whereas the deep convection case produces deep heating up to 14 km. Although the storm passage stabilizes the atmosphere in both cases, the congestus case has more instability in the mid-level, providing a more favorable condition for the next batch of convection to grow deep. The water vapor profiles show similar results. Both cases dry the boundary layer effectively. The drying continues up to about 4 km for the deep convection case. However, the congestus case quickly switches from drying to moistening at about 2 km. It remains a larger moisture source than the deep convection up to about 6 km. Above 6 km, deep convection acts as the moisture source up to the tropopause, whereas the congestus shows limited influence in both temperature and water vapor.

These model results agree with many previous observations on the roles of congestus in the tropics, especially in the context of the MJO lifecycle. The observations and analyses have shown that prior to the peak MJO phase, which is characterized by deep convection with large anvils, there is a gradual buildup of mid-tropospheric water vapor (e.g., Kemball-Cook and Weare 2001; Kiladis et al. 2005; Tian et al. 2006). This water vapor buildup is mainly attributed to the cumulus congestus population that leads to the peak phase (e.g., Masunaga et al. 2006; Lau and Wu 2010).

Our model simulations confirm the roles congestus play in moistening and destabilizing the mid-troposphere, setting up favorable conditions for the deep convection during the MJO's peak phase. A more significant and new aspect of this study is that variations in aerosol number concentrations alone could change the state of convection from the congestus dominant regime to deep convection dominant regime.

6. Summary and discussion

6.1 Summary

This study examines the significance of aerosol (serving as CCN) in modulating strengths of the tropical oceanic convection during a TOGA COARE convection period, with the focus on cumulus congestus population. The GCE cloud-resolving model with a spectral bin microphysical scheme is used to investigate how increasing the aerosol number concentration from the mean maritime background level can invigorate convection and shift the cloud population from the cumulus congestus dominant regime to deep convection regime. It is argued that over the tropical oceans, where water vapor is abundant, atmospheric instability is low, and a weak stable level often exists near the 0°C, the maritime background environment combined with a low aerosol concentration is conducive for the formation of congestus. The sensitivity tests that vary the initial cold pool strength, low-level wind shear, aerosol spectra, and the model horizontal resolution (not shown) show robust responses of convection invigoration when aerosol concentrations are raised from their clean, background values. Several mechanisms for convection invigoration by aerosol are identified and tested using model data and additional sensitivity tests. They include increased latent heat release by both condensation and freezing, enhanced cloud top evaporation, and increased downdrafts and cold pool strengths. Among these mechanisms, the enhanced latent heating in vapor condensation is probably the most important factor.

6.2 Discussions

In this section, we offer some general discussions on tropical convection that stemmed from this study. Although we feel this is a relevant and potentially important concept, it remains a hypothesis and much more work is required in the future.

The early theory on tropical clouds consists of two types: deep towers that reach the tropopause and small cumuli confined below the trade wind inversions (e.g., Simpson 1992). The radar observations have significantly expanded our understanding of tropical precipitation. On the basis of radar-observed cloud top height distributions, Johnson et al. (1999) proposed the tri-modal tropical convection, which added cumulus congestus to the earlier proposed theory by, e.g., Riehl and Malkus (1958). Figure 12 shows a schematic plot of the tri-modal convection with aerosol lifecycle added in the image. Note that the deep tower (the cumulonimbus in Fig. 12) has an extensive stratiform anvil attached. This stratiform region is important both dynamically and thermodynamically in the tropics (e.g., Houze 2004). The congestus population and stratiform region are complementary in terms of their flow patterns (mid-level outflow vs. mid-level inflow), as well as in their heating profiles (bottom heavy vs. top heavy). Furthermore, melting of ice phase particles in the stratiform region may contribute to the stability near the 0°C level in the tropics (Mapes and Zuidema 1996; Posselt et al. 2008). How different cloud populations form and evolve in the tropics remains an active research topic. In this study, we have added another layer of complication, i.e., maritime aerosols and their effects on convection intensity. The TOGA COARE case study has shown that clean background aerosol may help maintain the congestus population. In addition, we have introduced some speculations in Fig. 12 to show how different types of clouds might affect maritime aerosols' budget. The current GCE model does not include the full aerosol life cycle with all sources and sinks. However, this does not affect the conclusions in this study because we used open lateral boundary conditions. There is significant wet removal of aerosols in the precipitating area. However, the clean air mass generally leaves the convective system and does not participate in any new development. In the future, we plan to add the full maritime aerosol physics and chemistry in the cloud-resolving model in order to quantify the marine aerosol budget.

The spectrum of convection shown in Fig. 12 and their dynamical interactions pose a serious challenge in global climate simulations, where individual convection generally cannot be resolved. Modeling studies have shown large sensitivities in the general circulation models (GCMs) to different cumulus parameterization schemes. Nevertheless, improvements in cumulus parameterization that limit convection strengths in some way often led to better representations of the tropical convection and more realistic MJO signals. For example, Boyle et al. (2008) reported better forecasts for the TOGA COARE case when using a modified Zhang–McFarlane scheme with

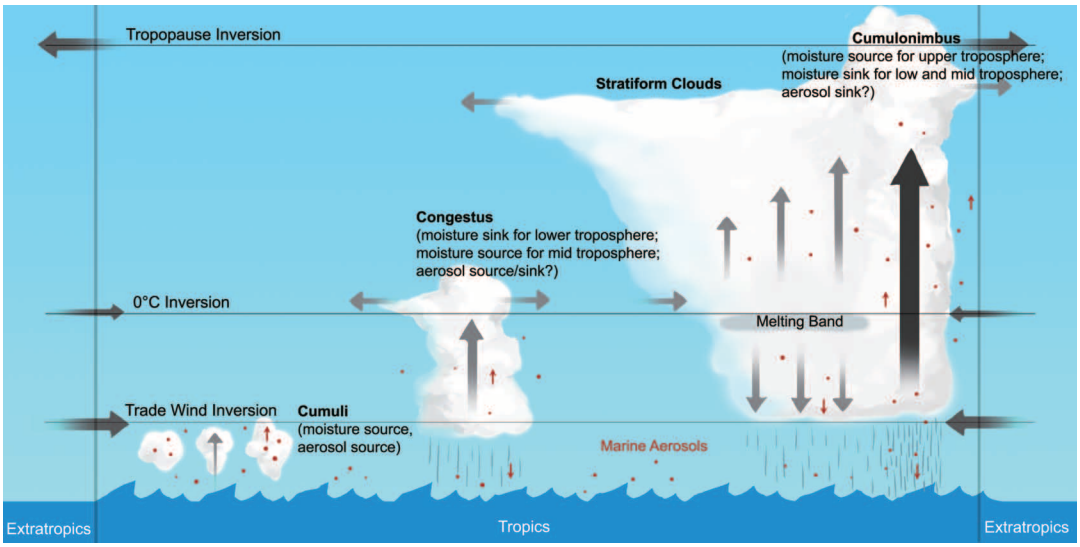

Fig. 12. North–south schematic view of the three inversion layers and their associated major cloud populations over the tropical oceans. The dark arrows indicate airflow directions and strengths. The red arrows indicate source (upward) and sink (downward) of marine aerosols associated with different clouds.

a relative humidity threshold for convection trigger in the community climate model (CAM3). Bechtold et al. (2008) found improved forecasting scores and more realistic spectrum of convectively coupled equatorial waves when the convective entrainment rate was adjusted on the basis of environmental humidity in the ECMWF Integrated Forecasting System. A superparameterized CAM3, where convection is explicitly resolved by a 2D cloud-resolving model within a GCM grid, produced better MJO signals than the original CAM3 (Thayer-Calder and Randall 2009). Moreover, the reason is attributed to the improved representations of the vertical distributions of water vapor. There is mounting evidence that some sort of convection "limiter" or "damper" is required in the GCMs to prevent the atmosphere from releasing its instability too quickly. This would allow for a gradual building up of moisture at the mid-troposphere, setting up conditions for deep convection episodes with extensive stratiform regions. Although the GCMs may simulate the "limiter" by, e.g., increasing the convection entrainment rate in the cumulus parameterization scheme, a clear picture of physical mechanisms is still missing.

On the basis of the modeling studies, we propose a physical mechanism that may act as a convection "limiter," i.e., the very low marine background aerosol concentrations. The model simulations show that the lack of marine aerosol serving as CCN may limit convection strengths and promote congestus formation. This hypothesis points to a possible mechanism for convection damping. This limiter also applies to the global cloud-resolving simulations. For example, with the superparameterization in a GCM, the convection still shows hyperactivity (Thayer-Calder and Randall 2009). Adding the damping effect related to low aerosol concentration over the tropical oceans may reduce this hyperactivity. Several studies are required, including both cloud-scale and global-scale modeling, as well as observational support, in order to make these speculations relevant. Understanding maritime aerosol lifecycles, moisture source/sink, as well as their interactions with different cloud types, are some of the key issues.

Acknowledgments

This research is mainly supported by NASA headquarters and the NASA PMM Mission. We thank two anonymous reviewers for their detailed suggestions that significantly improved the clarity of this manuscript. The first author wishes to thank Professor Rob Fovell of UCLA for helpful discussions, Amy Houghton of USRA, Lisa Nalborczyk, and Stephen Palm of SSAI for editing the manuscript, and Jenny Zeng for beautifully rendering Fig. 12. This study is dedicated to Joanne Simpson, who remains an

inspiration for many of us.

References

Bechtold, P., M. Kohler, T. Jung, F. Doblas-Reyes, M. Leutbecher, M. Rodwell, F. Vitart, and G. Balsamo, 2008: Advances in simulating atmospheric variability with the ECWMF model: From synoptic to decadal time-scales. *Quart. J. Roy. Meteor. Soc.*, **134**, 1337–1352.

Boyle, J., S. Klein, G. Zhang, S. Xie, and X. Wei, 2008: Climate model forecast experiments for TOGA COARE. *Mon. Wea. Rev.*, **136**, 808–832.

Fan, J., T. Yuan, J. Comstock, S. Ghan, A. Khain, L. Leung, Z. Li, V. Martins, and M. Ovchinnikov, 2009: Dominant role by vertical wind shear in regulating aerosol effects on deep convective clouds. *J. Geophys. Res.*, **114**, D22206, doi:10.1029/2009JD012352.

Fan, J., J. M. Comstock, M. Ovchinnikov, S. A. Mcfarlane, G. Mcfarquhar, and G. Allen, 2010: Tropical anvil characteristics and water vapor of the tropical tropopause layer: Impact of heterogeneous and homogeneous freezing parameterizations. *J. Geophys. Res.*, **115**, D12201, doi:10.1029/2009JD012696.

Fitzgerald, J. W., 1991: Marine aerosols: A review. *Atmos. Environ.*, **25A**, 533–545.

Folkins, I., S. Fueglistaler, G. Lesins, and T. Mitovski, 2008: A low-level circulation in the tropics. *J. Atmos. Sci.*, **65**, 1019−1034.

Folkins, I., 2009: A one-dimensional cloud model with trimodal convective outflow. *J. Climate*, **22**, 6437–6455.

Fovell, R. G., and P.-H. Tan, 2000: A simplified squall-line model revisited. *Quart. J. Roy. Meteor. Soc.*, **126**, 173–188.

Fridlind, A. M., A. S. Ackerman, J. P. Chaboureau, J. Fan, W. W. Grabowski, A. A. Hill, T. R. Jones, M. M. Khaiyer, G. Liu, P. Minnis, H. Morrison, L. Nguyen, S. Park, J. C. Petch, J. P. Pinty, C. Schumacher, J. B. Sipway, A. C. Varble, X. Wu, S. Xie, and M. Zhang, 2012: A comparison of TWP-ICE observational data with cloud-resolving model results. *J. Geophy. Res.*, **117**, D05204, doi:10.1029/2011JD016595.

Houze, R. A., 2004: Mesoscale convective systems. *Rev. Geophys.*, **42**, RG4003, doi:10.1029/2004RG000150.

Hudson, J. G., 1993: Cloud condensation nuclei near marine cumulus. *J. Geophy. Res.*, **98**, 2693–2702.

Jaenicke, R., 1993: Tropospheric aerosols. *Aerosol-Cloud-Climate Interactions*. Hobbs, P. V. (ed.), Academic Press, lnc., 1−31.

Jensen, M. P., and A. D. Del Genio, 2006: Factors limiting convective cloud-top height at the arm Nauru island climate research facility. *J. Climate*, **19**, 2105−2117.

Johnson, R. H., P. E. Ciesielski, and K. A. Hart, 1996: Tropical inversions near the 0 ˚C level. *J. Atmos. Sci.*, **53**, 1838–1855.

Johnson, R. H., T. M. Rickenbach, S. A. Rutledge, P. E. Ciesielski, and W. H. Schubert, 1999: Trimodal characteristics of tropical convection. *J. Climate*, **12**, 2397–2418.

Jorgensen, D. P., M. A. Lemone, and S. B. Trier, 1997: Structure and evolution of the 22 February 1993 TOGA COARE squall line: Aircraft observations of precipitation, circulation, and surface energy fluxes. *J. Atmos. Sci.*, **54**, 1961−1985.

Kemball-Cook, S. R., and B. C. Weare, 2001: The onset of convection in the Madden-Julian Osicllation. *J. Climate*, **14**, 780–793.

Khain, A., M. Ovtchinnikov, M. Pinsky, A. Pokrovsky, and H. Krugliak, 2000: Notes on the state-of-the-art numerical modeling of cloud microphysics. *Atmos. Res.*, **55**, 159–224.

Khain, A. P., N. Benmoshe, and A. Pokrovsky, 2008: Factors determining the impact of aerosols on surface precipitation from clouds: An attempt at classification. *J. Atmos. Sci.*, **65**, 1721−1748.

Kiladis, G. N., K. H. Straub, and P. T. Haertel, 2005: Zonal and vertical structure of the Madden-Julian Oscillation. *J. Atmos. Sci.*, **62**, 2790−2809.

Koren, I., G. Feingold, and L. A. Remer, 2010: The invigoration of deep convective clouds over the Atlantic: Aerosol effect, meteorology or retrieval artifact. *Atmos. Chem. Phys*, **10**, 8855−8872.

Lau, K.-M., and H.-T. Wu, 2010: Characteristics of precipitation, cloud, and latent heating associated with the Madden-Julian Oscillation. *J. Climate*, **23**, 504–518.

Lebo, Z. J., H. Morrison, and J. H. Seinfeld, 2012: Are simulated aerosol-induced effects on deep convective clouds strongly dependent on saturation adjustment? *Atmos. Chem. Phys.*, **12**, 9941–9964.

Lemone, M. A., E. J. Zipser, and S. B. Trier, 1998: The role of environmental shear and thermodynamic conditions in determining the structure and evolution of mesoscale convective systems during TOGA COARE. *J. Atmos. Sci.*, **55**, 3493–3518.

Lin, J., B. E. Mapes, M. Zhang, and M. Newman, 2004: Stratiform precipitation, vertical heating profiles, and the Madden-Julian Oscillation. *J. Atmos. Sci.*, **61**, 296–309.

Luo, Z., G. Y. Liu, G. L. Stephens, and R. H. Johnson, 2009: Terminal versus transient cumulus congestus: A CloudSat perspective. *Geophy. Res. Lett.*, **36**, L05808, doi:10.1029/2008GL036927.

Mapes, B. E., and P. Zuidema, 1996: Radiative-dynamical consequences of dry tongues in the tropical troposphere. *J. Atmos. Sci.*, **53**, 620−638.

Masunaga, H., T. S. L'Ecuyer, and C. Kummerow, 2005: Variability in the characteristics of precipitation systems in the tropical Pacific. Part I: Spatial structure. *J. Climate*, **18**, 823−838.

Masunaga, H., T. L'ecuyer, and C. Kummerow, 2006: The Madden–Julian Oscillation recorded in early observations from the tropical rainfall measuring mission (TRMM). *J. Atmos. Sci.*, **63**, 2777–2794.

Masunaga, H., 2009: A 9-season TRMM observation of the austral summer MJO and low-frequency equatorial waves. *J. Meteor. Soc. Japan*, **87A**, 295.

Meyers, M. P., P. J. De Mott, and W. R. Cotton, 1992: New primary ice–nucleation parameterizations in an explicit cloud model. *J. Appl. Meteor.*, **31**, 708–721.

Morrison, H., and W. W. Grabowski, 2011: Cloud-system resolving model simulations of aerosol indirect effects on tropical deep convection and its thermodynamic environment. *Atmos. Chem. Phys*, **11**, 10503–10523.

Pachauri, R. K., and A. Reisinger, 2007: *Climate Change 2007: Synthesis Report*. Contribution of working groups I, II and III to the fourth assessment report of the Intergovernmental Panel on Climate Change. IPCC, 104 pp.

Posselt, D. J., S. C. Van Den Heever, and G. L. Stephens, 2008: Trimodal cloudiness and tropical stable layers in simulations of radiative convective equilibrium. *Geophy. Res. Lett.*, **35**, L08802, doi:10.1029/2007GL033029.

Reutter, P., H. Su, J. Trentmann, M. Simmel, D. Rose, S. S. Gunthe, H. Wernli, M. O. Andreae, and U. Poschl, 2009: Aerosol- and updraft-limited regimes of cloud droplet formation: Influence of particle number, size and hygroscopicity on the activation of cloud condensation nuclei (CCN). *Atmos. Chem. Phys.*, **9**, 7067−7080.

Riehl, H., and J. S. Malkus, 1958: On the heat balance of the equatorial trough zone. *Geophysica*, **6**, 503–538.

Rosenfeld, D., U. Lohmann, G. B. Raga, C. D. O'Dowd, M. Kulmala, S. Fuzzi, A. Reissell, and M. O. Andreae, 2008: Flood or drought: How do aerosols affect precipitation? *Science*, **321**, 1309–1313.

Rotunno, R., J. B. Klemp, and M. L. Weisman, 1988: A theory for strong, long-lived squall lines. *J. Atmos. Sci.*, **45**, 463−485.

Simpson, J., 1992: Global circulation and tropical cloud activity. *The Global Role of Tropical Rainfall*. Theon, J. S. et al. (eds.), A. Deepak Publishing, 77–92.

Smolarkiewicz, P. K., and W. Grabowski, 1990: The multidimensional positive advection transport algorithm: Nonoscillatory option. *J. Comput. Phys.*, **86**, 355–375.

Storer, R. L., and S. C. van den Heever, 2013: Microphysical processes evident in aerosol forcing of tropical deep convective clouds. *J. Atmos. Sci.*, **70**, 430–446.

Tao, W.-K., X. Li, A. Khain, T. Matsui, and S. Lang, 2007: Role of atmospheric aerosol concentration on deep convective precipitation: Cloud-resolving model simulations. *J. Geophys. Res.*, **112**, doi:10.1029/2007JD008728.

Tao, W.-K., J.-P. Chen, Z. Li, C. Wang, and C. Zhang, 2012: Impact of aerosols on convective clouds and precipitation. *Rev. Geophys.*, **50**, D24S18, doi:10.1029/2011RG000369.

Thayer-Calder, K., and D. A. Randall, 2009: The role of convective moistening in the Madden-Julian Oscillation. *J. Atmos. Sci.*, **66**, 3297–3312.

Tian, B., D. E. Waliser, E. J. Fetzer, B. H. Lambrigtsen, Y. L. Yung, and B. Wang, 2006: Vertical moist thermodynamic structure and spatial-temporal evolution of the MJO in AIRS observations. *J. Atmos. Sci.*, **63**, 2462–2485.

Trier, S. B., W. C. Skamarock, M. A. Lemone, D. B. Parsons, and D. P. Jorgensen, 1996: Structure and evolution of the 22 February 1993 TOGA COARE squall line: Numerical simulations. *J. Atmos. Sci.*, **53**, 2861–2886.

Twomey, S., and T. A. Wojciechowski, 1969: Observations of the geographical variation of cloud nuclei. *J. Atmos. Sci.*, **26**, 684–688.

Van Den Heever, S. C., G. L. Stephens, and N. B. Wood, 2011: The impacts of enhanced cloud condensation nuclei concentrations on tropical convection characteristics under conditions of radiative convective equilibrium. *J. Atmos. Sci.*, **68**, 699−718.

Wang, C., 2005: A modeling study of the response of tropical deep convection to the increase of cloud condensation nuclei concentration: 1. Dynamics and microphysics. *J. Geophys. Res.*, **110**, D21211, doi:10.1029/2004JD005720.

Wang, Y., W.-K. Tao, J. Simpson, and S. Lang, 1996: The impact of a surface layer on a TOGA COARE cloud system development. *Mon. Wea. Rev.*, **124**, 2753–2763.

Wang, Y., W.-K. Tao, J. Simpson, and S. Lang, 2003: The sensitivity of tropical squall lines to surface fluxes: Three-dimensional cloud resolving model simulations. *Quart. J. Roy. Meteor. Soc*, **129**, 987–1006.

Weisman, M. L., J. B. Klemp, and R. Rotunno, 2004: "A theory for strong long-lived squall lines" revisited. *J. Atmos. Sci.*, **61**, 361−382.

Yin, Y., K. S. Carslaw, and G. Feingold, 2005: Vertical transport and processing of aerosols in a mixed-phase convective cloud and the feedback on cloud development. *Quart. J. Roy. Meteor. Soc.*, **131**, 221−245.

Yuan, T., L. A. Remer, K. E. Pickering, and H. Yu, 2011: Observational evidence of aerosol enhancement of lightning activity and convective invigoration. *Geophys. Res. Lett.*, **38**, L04701, doi:10.1029/2010GL046052.